Journal of Hydrology 587 (2020) 124902

Contents lists available at ScienceDirect

Journal of Hydrology

journal homepage: www.elsevier.com/locate/jhydrol

Research papers

Understanding the re-infiltration process to simulating streamflow in North Central Texas using the WRF-hydro modeling system

Jiaqi Zhang[a], Peirong Lin[b], Shang Gao[c], Zheng Fang[a,*]

[a] Department of Civil Engineering, University of Texas at Arlington, Arlington, TX, USA
[b] Department of Civil Engineering, Princeton University, Princeton, NJ, USA
[c] Department of Civil Engineering, University of Oklahoma, Norman, OK, USA

ARTICLE INFO

Keywords:
WRF-Hydro
Run-on
Re-infiltration
Calibration
Saturated hydraulic conductivity
REFKDT
Runoff coefficient

ABSTRACT

WRF-Hydro (Weather Research and Forecasting model-Hydrological modeling system), as the core engine of the United States National Water Model (NWM), has now been used in many hydrometeorological applications throughout the world. One important feature that WRF-Hydro introduced is to allow infiltration excess ("ponded water") for subsequent lateral re-distribution and soil re-infiltration, which is a major enhancement in terms of physical realism. Nonetheless, how well WRF-Hydro models re-infiltration is largely unknown, because this process is difficult to be directly measured. To gain an in-depth understanding of re-infiltration process under different hydrometeorological/geographical conditions with model parameter settings, we start conducting a series of idealized numerical experiments using 18 watersheds in North Central Texas as a testbed. Next, the model is automatically calibrated to best quantify re-infiltration amounts during two major storms (2010 Tropical Storm Hermine and 2015 May Event), which is accomplished by coupling the dynamically dimensioned search (DDS) algorithm with WRF-Hydro to achieve optimal calibration efficiency. The results show that re-infiltration has quite substantial impacts on streamflow simulation in WRF-Hydro, especially for areas with flat terrains and soils with high clay content. Among all examined factors, precipitation, saturated hydraulic conductivity (K_{sat}) and runoff partition parameter (REFKDT) are found to impose relatively higher impacts on both re-infiltration ratio and runoff coefficient. It is also found that the runoff coefficient and the re-infiltration ratio are positively correlated based on results from both hypothetical and real events, indicating re-infiltration effects can become more pronounced as flood potential increases. These findings collectively show the significance of representing the re-infiltration process in flood forecasting. Models that do not incorporate this process may be over-calibrated to compensate errors originated from the missing process.

1. Introduction

Flooding is the most frequent weather hazard that can cause serious fatalities and property damages (Morrs, 2010; Deb et al., 2018). Extreme weather and the impacts of climate change are expected to increase the frequency and severity of flood events globally (IPCC, 2014). To provide early warnings and improve the emergency response for floods, the National Water Model (NWM), a continental-scale high-resolution hydrologic forecasting system for the United States, has been brought into operations in August of 2016 (NOAA, 2016). This hydrologic forecasting system simulates discharge for 2.7 million NHDPlus (National Hydrography Dataset Plus) stream reaches and extends the watershed hydrology to continental hydrology (Maidment, 2017; Lin et al., 2017). The NWM is developed from the community-based WRF-Hydro model (Gochis et al., 2013), an architectural framework which couples the Noah land surface model (LSM) with multi-parameterization (Noah-MP; Niu et al., 2011) with atmospheric models and hydrological routing schemes. Since its operational use in the NWM, WRF-Hydro has been tested and applied in different regions throughout the world for a range of applications in predicting runoff/streamflow (Gochis et al., 2015; Senatore et al., 2015), floods (Yucel et al., 2015; Lin et al., 2018a; Lin et al., 2018b), and land–atmosphere feedbacks (Arnault et al., 2015).

While the enclosed Noah and Noah-MP components simulate the one-dimensional (1-D) soil–vegetation–atmosphere interactions between surface and atmosphere (Gochis and Chen 2003), WRF-Hydro further extends the calculation of the surface overland flow, saturated subsurface flow, channel routing, and baseflow processes on a 2-D gridded planar surface (Gochis et al., 2013). Prior to being transformed to overland flow, surface runoff in WRF-Hydro is described as

* Corresponding author.
E-mail address: nickfang@uta.edu (Z. Fang).

https://doi.org/10.1016/j.jhydrol.2020.124902
Received 7 December 2019; Received in revised form 11 March 2020; Accepted 26 March 2020
Available online 29 March 2020

infiltration excess while subsurface runoff is the vertical drainage accumulated at the bottom of the soil column. Other hydrological components, which are not the focus of this study, include throughfall, direct soil evaporation, transpiration, re-evaporation of precipitation intercepted by the canopy, vertical soil water movement and a simple lake/reservoir routing scheme (Ek et al., 2003). In this study, we are particularly interested in one major enhancement that WRF-Hydro introduces, which is to allow the infiltration excess to remain as "ponded water" for subsequent lateral re-distribution in combination with precipitation in the following model time step (Yucel et al., 2015). When ponded water starts to move downslope as overland flow, an important process previously known as the "run-on" effect (Smith and Hebbert, 1979) will occur. The "run-on" process can be defined as the surface water running from the upstream areas on downslope areas where moisture deficit has not yet been satisfied (Corradini et al., 1998; Nahar, et al., 2004). In addition to the direct infiltration caused by rainfall-runoff process in the vertical direction, this "run-on" process can also be viewed as re-infiltration due to the runoff re-distribution (Güntner and Bronstert, 2004). Hereafter, we use the word "re-infiltration" to refer to this process for simplicity.

Previous studies using field/numerical experiments have observed that re-infiltration can cause a decrease in unit area runoff as watershed size increases (Yair and Kossovsky, 2002; Yair and Raz-Yassif, 2004; Gomi et al., 2008; Heras et al., 2010). Woolhiser et al. (1996) conducted numerical experiments and found that re-infiltration has a major impact on runoff peaks, volumes and time to peak as saturated hydraulic conductivity (K_{sat}) increases downslope. Nahar et al. (2004) examined the role of run-on process on field-scale infiltration and one-dimensional overland flow using analytical models and Monte-Carlo simulations. They found that field-scale mean of infiltration would increase in the presence of run-on, which in turn affects the hydrograph. Corradini et al. (1998, 2002) suggests the re-infiltration process cannot be disregarded especially when the spatial randomness of soil properties is taken into account in hydrologic modeling as it produces a significant decrease in overland flow.

As an influencing factor to the re-infiltration process, K_{sat} has been the focal point in numerous previous studies investigating its heterogeneous effect on this process (e.g. Smith and Hebbert, 1979; Saghafian et al., 1995; Woolhiser et al., 1996; Nahar et al., 2004). Saghafian et al. (1995) solved the diffusive wave equations and Green-Ampt infiltration equation to examine the impacts of K_{sat} spatial variability, where they concluded strong sensitivity of runoff volume and peak to this parameter. Corradini et al. (1998, 2002) evaluated run-on effects under conditions of horizontal heterogeneity of K_{sat} using a model with kinematic wave approximation and conceptual infiltration approach, where they found the level of spatial correlation in K_{sat} is less important when the overland flow volume was appreciable. Nahar et al. (2004) found re-infiltration is less important when the ratio of rainfall intensity to K_{sat} is large. Besides K_{sat} and precipitation, other hydrometeorological and geographic conditions such as soil moisture saturation degree, terrain slope as influencing factors to re-infiltration have been largely understudied.

As powerful remote sensors and computers became available, hydrologic community developed complex distributed models that can represent the dominant hydrological processes and their interactions (e.g., Rigon et al., 2006; Qu and Duffy, 2007; Lawrence et al., 2011; Niu et al., 2011). Like WRF-Hydro, many incorporate re-infiltration processes, e.g. DHSVM, (Wigmosta et al., 1994), Tethys-Chloris (Fatichi et al., 2012), Ech2O (Maneta and Silverman, 2013). However, WRF-Hydro has the option to disable "re-infiltration" function, which enables us to conduct numerical experiments with/without re-infiltration. Moreover, as a community model, WRF-Hydro is a platform for all users to share insights on hydrologic processes. The improved understanding in the WRF-Hydro framework promises to enhance the performance of the National Water Model. Therefore, we are motivated to comprehensively investigate the role of re-infiltration with regard to streamflow simulation by leveraging WRF-Hydro as the ideal modeling platform.

In this paper, the authors seek to systematically answer the following questions: (1) How do different hydrometeorological conditions such as the intensity of precipitation, soil moisture levels affect re-infiltration? (2) How do different geographic conditions such as digital elevation model (DEM)/terrain slope, roughness, soil type influence re-infiltration? (3) How do model parameters impact the re-infiltration process? (4) What is the role of re-infiltration in real storm events and how important is it?

The paper is organized as follows: Section 2 describes the methodology in detail, including the study area, model configurations, simulations, and calibrations; the results with discussions are presented in Section 3; Section 4 provides the conclusions and insights gained from this study.

2. Methodology

2.1. Study area and model configurations

The Upper Trinity River Basin (UTRB) is located in the North Central Texas with 16,602 km^2. Undeveloped portion of the land constitutes a large percentage of UTRB (Fig. 1**A**), which makes infiltration loss a vital component in the regional hydrologic cycle. Moreover, sitting in a region of temperate mean climatological conditions (USACE, 2013), UTRB experiences occasional extremes of temperature and precipitation with relatively short duration. The complexity of infiltration process and climate variability imposes challenges to water resources engineering practices like flow frequency analysis and flood forecasting. Fig. 1**B** shows the configuration of domain with Digital

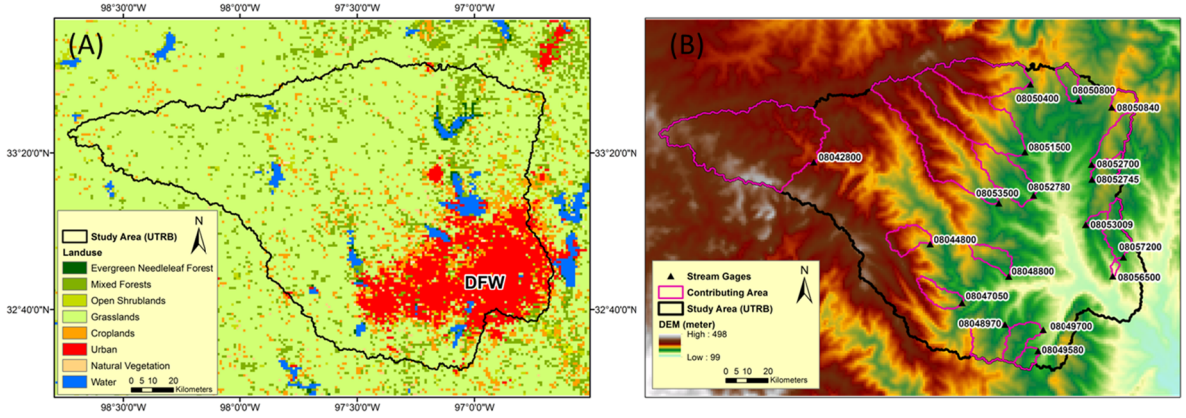

Fig. 1. . Study area and modeling domain. (A) Land use type. (B) Digital Elevation Model (DEM) and stream gauges with corresponding contributing area.

Elevation Model (DEM) and the locations of USGS stream gauges with corresponding contribution areas.

The complete description of the WRF-Hydro system version 5.0 can be found in Gochis et al. (2018). While the Noah-MP LSM provides several physical parameterizations, the same surface runoff option (free drainage) adopted by the NWM is used, where vertical surface runoff is calculated as excess water after precipitation supply infiltrates into the soil (Schaake et al. 1996). Within soil column (2 m deep), Richards equation is deployed for infiltration of four layers, which have the thicknesses of 10, 30, 60, and 100 cm, respectively. Other hydrological processes are described in Niu et al. (2011), Yang et al. (2011), Cai et al. (2014), and Zheng and Yang (2016). A fully-unsteady, explicit diffusive wave formulation (Julien et al., 1995; Ogden, 1997) with steepest descent approach is deployed to solve overland flow routing. Subsurface lateral flow is calculated prior to overland flow, which allows exfiltration from fully saturated grid cells to be added to the infiltration excess calculated from the LSM (Senatore et al., 2015; Gochis et al., 2018). In order to represent overland and subsurface flow processes on higher spatial resolution, the subgrid disaggregation-aggregation routines are used right after the main LSM loop and before the surface/subsurface routing loop; details are described in Gochis and Chen (2003). This study uses 1 km (in total 159×259 grid cells) and 100 m resolution for the LSM and hydrologic routing grids, respectively, with an aggregation factor of 10. Channel routing is solved using a variable-parameter Muskingum–Cunge (MC) method (see Gochis et al. 2018 for channel shape parameters used).

To allow for the flexibility to dismiss the re-infiltration process and simplify the use of related parameters, terrain routing can be turned off in WRF-Hydro as a namelist switching feature. Physically, the terrain-on and terrain-off scenarios in the model are illustrated in Fig. 2. In terrain-on case (left), water available for infiltration includes both precipitation and overland surface runoff from upslope areas. While in terrain-off scenario (right), infiltration is caused by precipitation alone; hereafter, this process is referred as "local infiltration" (Corradini et al., 1998) to be differentiated from re-infiltration. With re-infiltration switched off, any infiltration excess is routed downstream without having chance to re-enter the soil columns, meaning local infiltration only; while the terrain-on scenario includes both local infiltration and re-infiltration. Switching on/off of this setting in WRF-Hydro allows us to perform a series of experiments to investigate and quantify re-infiltration.

Table 1
Description of idealized forcing input.

Variable Name	Range and Unit of Values	Timing
Shortwave radiation	0–900 W/m^2	Diurnal cycle
Longwave radiation	375–425 W/m^2	Diurnal cycle
Specific humidity	0.01 kg/kg	Constant
Air temperature	287–293 K	Diurnal cycle
Surface pressure	100,000 Pa	Constant
Wind speed at u direction	1.0 m/s	Constant
Wind speed at v direction	1.0 m/s	Constant

2.2. Model experiments

We first conduct a series of idealized modeling experiments under different hydrometeorological, geographical conditions, and model parameters. Before each model run, a 1.5-month spin-up is conducted to achieve model equilibrium states which is considered appropriate for flood simulations with thin soils in Texas (Lin et al., 2018a; Lin et al., 2018b). Except for the experiments focusing on precipitation, other experiments all use 50.8 mm (2 in.) precipitation with 1-h duration. The amount of precipitation is chosen because it is approximately equivalent to a five-year storm as outlined in North Central Texas Council of Government integrated Stormwater Management Technical Hydrology Manual (NCTCOG iSWM, 2010). Other forcing variables (incoming shortwave and longwave radiation, specific humidity, air temperature, surface pressure and near surface u- and v-wind) are set to reflect idealized conditions, which have either constant values in space and time or a fixed diurnal cycle (Gochis et al., 2018). The detailed forcing information can be found in Table 1. For each experiment, we conduct a 48-h model run to ensure adequate time for water to flow from upstream to the outlet. In total, we conduct 9 sets of idealized modeling experiments with 150 runs.

2.2.1. Hydrometeorological conditions

Table 2 shows the experimental design for varying input precipitation values and initial soil moisture. The precipitation is applied

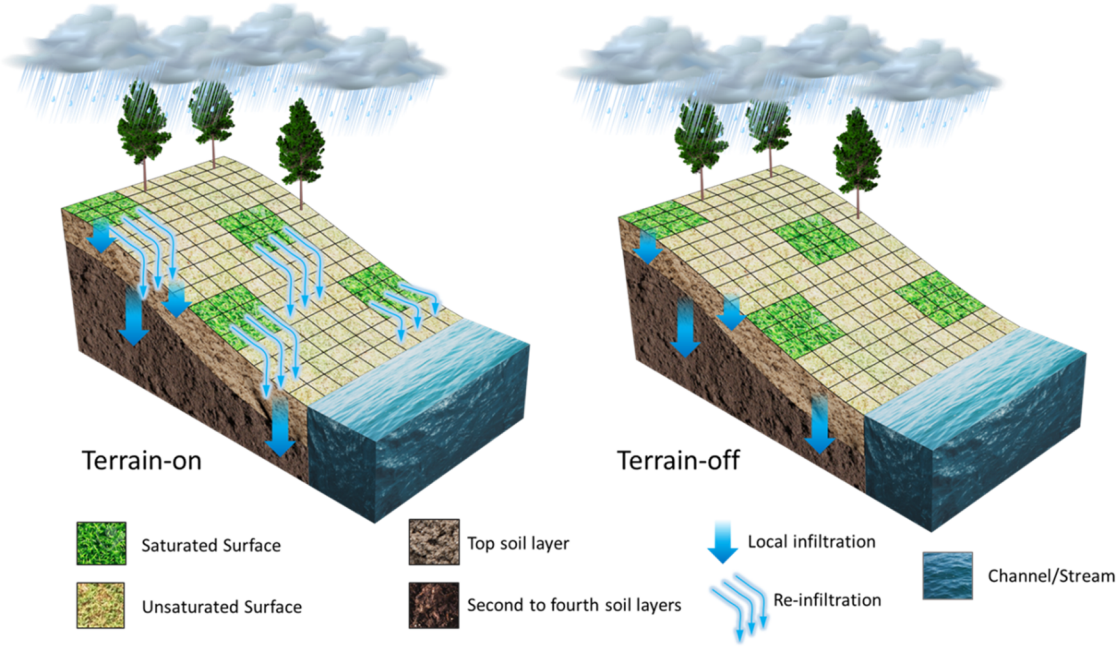

Fig. 2. . Illustration of mechanisms for terrain-on and terrain-off scenarios in WRF-Hydro.

Table 2
Experimental design for precipitation input and initial soil moisture condition.

Setting		Unit	Values
Precipitation		mm	12.7, 25.4, 38.1, 50.8, 63.5, 76.2, 88.9, 101.6, 114.3, 127
Initial soil moisture	First layer	$m^3\ m^{-3}$	Multiply maximum soil moisture by 0.2, 0.4, 0.6, 0.8, 1.0
	Second layer	$m^3\ m^{-3}$	Multiply maximum soil moisture by 0.2, 0.4, 0.6, 0.8, 1.0
	Third layer	$m^3\ m^{-3}$	Multiply maximum soil moisture by 0.2, 0.4, 0.6, 0.8, 1.0

for a 1-h duration during the first hour of simulation with a total amount of 12.7 mm (0.5 in.) to 127 mm (5 in.), and the same precipitation is uniformly spread for the entire study area. Precipitation amount with 127 mm (5 in.) is approximately equivalent to a 500-year storm in the study region, which is set as the upper limit to cover all possible precipitation scenarios. For initial soil moisture, different saturation levels are applied to the top three soil layers (0–10 cm, 10–40 cm, and 40–100 cm) based on each grid cell's soil type at the start of each model simulation. Changing the saturation of the fourth layer (100–200 cm) is not included because saturating the fourth layer will lead to unrealistically high runoff amount (not shown here), due to the fact that Texas is dominated by thin soils with less than 1 m (Furl et al., 2018; Lin et al., 2018a). Therefore, it would be physically unreasonable to investigate the model sensitivity to the saturation level in the fourth soil layer.

2.2.2. Geographical conditions

The experimental design for varying terrain slope and saturated hydraulic conductivity (K_{sat}) is shown in Table 3. Terrain slope is modified by changing the digital elevation model (DEM) underlying the model simulation. The terrain slope of study basins ranges from 0.31% to 1.12% with an average of 0.64%, and different multipliers were applied to change the terrain slope. Various multiplication factors are also uniformly applied for K_{sat} in each grid cell.

2.2.3. Model parameters

Five empirical model parameters are selected for sensitivity analyses based on literature review (Senatore et al., 2015; Yucel et al., 2015; Silver et al., 2017; Kerandi et al., 2018), which includes REFKDT, RETDEPRTFAC, LKSATFAC, OVROUGHRTFAC, and SLOPE. These five parameters are unitless, often with no interpretable physical meaning, and are suggested to be adjusted through model calibration. Even in a physically-based model like WRF-Hydro, these physically-insignificant parameters are also unavoidable, which is resulted from our inability to model all processes (Wagener and Montanari, 2011) hampering our understanding on other physically-based process components. Therefore, these parameters are carefully studied here.

REFKDT (K_{dtref}) is a constant parameter used with REFDK (K_{ref}), which corresponds to the saturation hydraulic conductivity for silty clay loam. Niu (2011) documented that REFKDT can significantly influence surface infiltration and partition of total runoff into surface and subsurface runoff, where increasing REFKDT leads to decrease in surface runoff (Schaake et al., 1996; Niu, 2011). The equation involving REFKDT (K_{dtref}) is

$$K_{dt} = K_{dtref} \times \frac{K_{sat}}{K_{ref}} \tag{1}$$

where K_{sat} is saturated hydraulic conductivity, K_{ref} is saturated hydraulic conductivity for silty clay loam, and K_{dt} is a constant for calculating the maximum soil infiltration rate (I_{max}):

$$I_{max} = \frac{P \times \left\{\frac{d_{tot} \times [1 - e^{(-K_{dt} \times \Delta t)}]}{P + d_{tot} \times [1 - e^{(-K_{dt} \times \Delta t)}]}\right\}}{\Delta t} \tag{2}$$

where P is the effective precipitation intensity, d_{tot} is the total soil water depth (m) and Δt is the duration of time step.

RETDEPRTFAC, LKSATFAC, and OVROUGHRTFAC are multipliers for surface retention depth, lateral saturated hydraulic conductivity, and overland roughness, respectively. SLOPE is a coefficient for deep drainage. They have been documented in previous studies as sensitive parameters for runoff simulation, thus are chosen in this study. Table 4 shows the experiment values for the model parameters; the default values of these parameters are globally uniform. The experiments are conducted by varying one parameter while keeping the others as default values. It should be noted that default parameters are the same as those used in the operational NWM. Compared to other random parameter sets, they can reveal how WRF-Hydro would behave due to change of a single parameter or input, which will provide benefits of improving NWM's performance in the study region. In addition, the experiments are helpful to common users of WRF-Hydro who would use these default parameter values as a starting point in hydrologic simulations.

Table 3
Experimental design for terrain slope and saturated hydraulic conductivity.

Setting	Unit	Values
Terrain slope	%	Multiply by 1, 2, 4, 6, 8, 10, 20
Saturated hydraulic conductivity	m/s	Multiply by 0.1, 0.5, 1.0, 1.5, 2.0, 2.5, 3, 4, 5

Table 4
Experimental design for model parameters.

Parameters	Unit	Min	Max	Default	Values
REFKDT	—	0.5	5	3	0.5, 0.6, 0.7, 0.8, 0.9, 1, 1.5, 2, 3, 4, 5
RETDEPRTFAC	—	0	10	1	0, 1, 2, 4, 6, 8, 10
LKSATFAC	—	10	10,000	1000	10, 100, 500, 1000, 5000, 10,000
OVROUGHRTFAC	—	0.1	5	1	0.1, 0.5, 1, 2, 3, 4, 5
SLOPE	—	0.1	1	0.1	0.1, 0.5, 1

2.3. Real case simulation and calibration

WRF-Hydro is configured in an "offline" mode (hydro components do not feedback to WRF) for two real case simulations: 2010 tropical storm Hermine (Sep 8th, 2010) and 2015 May storm (May 28th, 2015). To ensure adequate spin-up time, the model is initialized on July 1st, 2010 and April 1st, 2015, respectively, leaving about 1.5–2 months for model to spin-up. The soil in Texas is relatively thin – up to 40 cm to 60 cm (Lin et al., 2018a; Furl et al., 2018), so 1.5–2 months spin-up is considered appropriate for flood simulations using WRF-Hydro. The North American Land Data Assimilation System (NLDAS-2) forcing variables and the National Centers for Environmental Prediction (NCEP) quality-controlled Stage IV precipitation estimates are utilized as the input meteorological forcings. Fig. 3 shows the spatial pattern of cumulative precipitation amounts for these two storm events by 4-km Stage IV product.

To obtain the best estimates of the local infiltration and re-infiltration amounts during the selected storm events, WRF-Hydro is calibrated with terrain-routing for 18 USGS stream gauges (Fig. 1**B**). We utilize the dynamically dimensioned search (DDS) algorithm (Tolson and Shoemaker, 2007) for calibrations, because it was demonstrated to be suitable for computationally expensive and spatially-distributed models. Compared to other algorithms, DDS converges faster and can

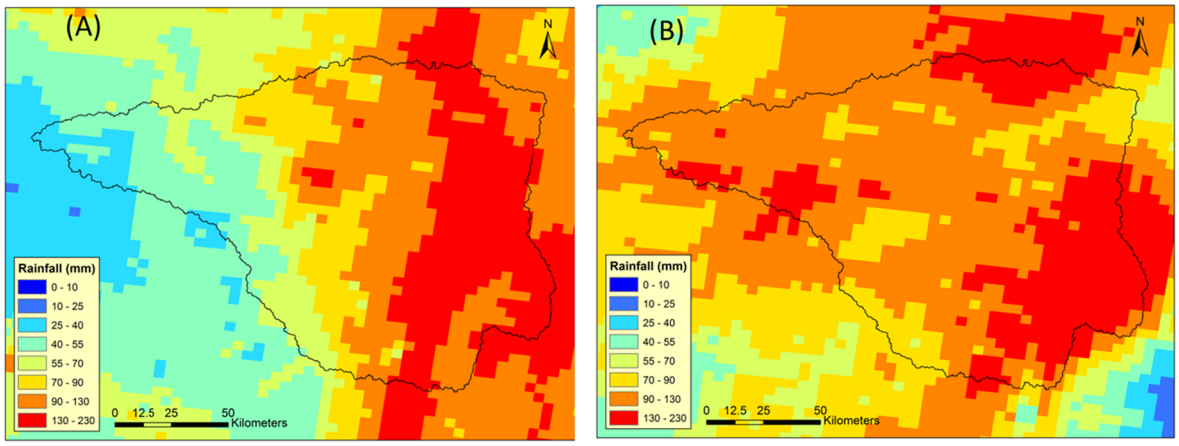

Fig. 3. . Cumulative precipitation amount from Stage IV estimates. (A) 2010 Tropical Storm Hermine (9/8/2010 00:00 UTC – 9/10/2010 23:00 UTC). (B) 2015 May Event (5/28/2015 00:00 UTC – 5/30/2015 23:00 UTC).

reach good global solutions within certain iterations (Tolson and Shoemaker, 2007). In a nutshell, DDS starts from a global search then switches to a more local search by dynamically adjusting the dimension of parameters; the adjustment from global to local search is achieved by dynamically and probabilistically reducing the number of dimensions in the neighborhood (Tolson and Shoemaker, 2007). To further expedite calibration, the simulation domain is reconfigured such that it is tailored to the 18 contributing basins towards all evaluation USGS gauges. The reduced simulation domain significantly shortens runtime per iteration, which allows us to assign a relatively large iteration number for improving calibration results. Lespinas et al. (2018) presents that the improvements in minimizing objective function using DDS are notable between 100 and 500 iterations and relatively moderate after 500 iterations. In terms of the objective function, Root-Mean-Square-Error (RMSE) indicates the magnitude of errors (streamflow difference) in time series between the simulated and observed hydrographs (Gupta et al., 2009). Based on the recommended information from previous studies, 500 iterations of DDS are used in the calibration with an objective function to minimize RMSE.

2.4. Hydrologic metrics

2.4.1. Re-infiltration calculation

Re-infiltration amount is not a direct output from WRF-Hydro, but can be estimated by subtracting local infiltration value from total infiltration value (Eq. (3)).

$$\text{Re} - \text{infiltration(mm)} = \text{Total infiltration(mm)} - \text{Local infiltration(mm)} \quad (3)$$

Based on the principle of water balance and considering negligible evapotranspiration during intense storm events, total infiltration can be calculated by subtracting runoff volume from precipitation amount in terrain-on simulation; local infiltration can be calculated by subtracting runoff volume from precipitation amount in terrain-off scenario. It should be noted that this relationship is not hard-coded into any part of WRF-Hydro, thus the re-infiltration is not calculated as residual of total infiltration subtracting local infiltration in the model. This is simply a way to interpret the total infiltration as a composite effect of two processes (local- and re-infiltration). Re-infiltration ratio is defined as re-infiltration amount divided by total infiltration. In some occasions, re-infiltration ratio can be greater than one, and this is interpreted as surface exfiltration occurring from saturated soil columns (Gochis et al., 2018).

2.4.2. Runoff coefficient

Runoff coefficient has been widely used in hydrologic practices, ranging from flood frequency analyses (e.g. Gottschalk and Weingartner, 1998; Sivapalan et al., 2005) to flood forecasting (e.g. Borga et al., 2011). For a given storm event, runoff coefficient is defined as the portion of precipitation that becomes direct runoff. Higher (lower) runoff coefficient indicates more (less) flood proneness, and it is used to understand its relationship with re-infiltration ratio.

2.4.3. Calibration statistics

Four statistics are used to evaluate the streamflow simulation results, including Pearson Correlation Coefficient (CC), Nash-Sutcliffe Efficiency (NSE), Root-Mean-Square-Error (RMSE), and Normalized Bias (NBIAS) (Eqs. (4)–(7)).

$$CC = \frac{cov(Q_{obs}, Q_{mod})}{\sigma_{obs}\sigma_{mod}} \quad (4)$$

$$NSE = 1 - \frac{\sum_{i=1}^{n}(Q_{mod}^{i} - Q_{obs}^{i})^2}{\sum_{i=1}^{n}(Q_{obs}^{i} - \bar{Q_{obs}})^2} \quad (5)$$

$$RMSE = \sqrt{\sum_{i=1}^{n}(Q_{mod}^{i} - Q_{obs}^{i})^2 / n} \quad (6)$$

$$NBIAS = \frac{\sum_{i=1}^{n}(Q_{mod}^{i} - Q_{obs}^{i})}{\sum_{i=1}^{n} Q_{obs}^{i}} \quad (7)$$

where Q_{mod} and Q_{obs} denote the simulation and observation values, *cov* is the covariance, σ_{obs} and σ_{mod} represent standard deviation of the simulation and observation; $\sum_{i=1}^{n}$means to sum up each time step from i = 1 to n, and n is the number of time steps.

Each of these metrics is interpreted differently to facilitate a more comprehensive understanding of the model performance. CC (Eq. (4)) measures how strong a co-varying relationship is between the modeled results and the observation, which cannot be used to assess model biases. NSE (Eq. (5)) and RMSE (Eq. (6)) are two most commonly used criteria in hydrological evaluations, and they measure both the variability of time series and the magnitude of errors (Gupta et al., 2009). NSE normalizes the squared model error, using the variance of the observed data, and thus a value of zero suggests that the model is only as good as the mean observed data, while NSE = 1 suggests perfect model simulation and negative values indicate that the observation mean is a better predictor than the model (Gupta and Kling, 2011). NBIAS (Eq. (7)) is calculated to identify both the magnitude and the sign of errors as normalized by the mean of the observations.

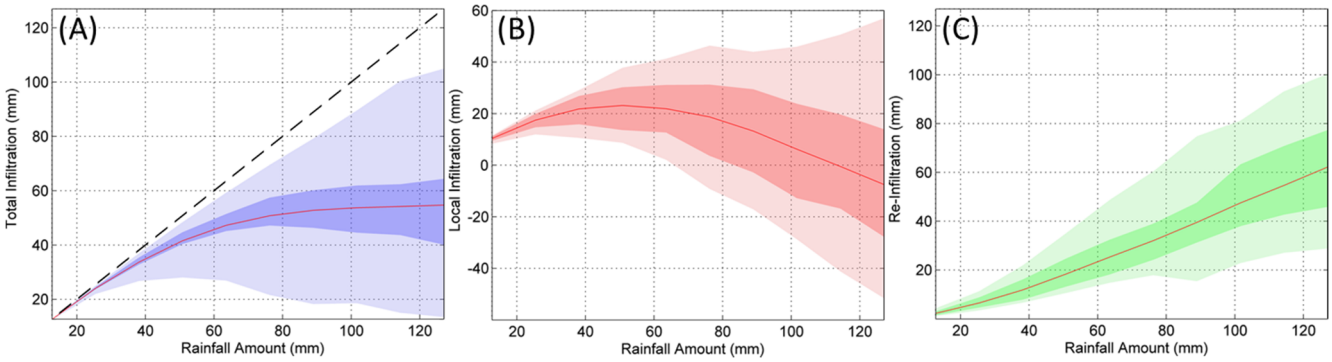

Fig. 4. . The range, interquartile range, and median value of (A) total infiltration, (B) local infiltration, and (C) re-infiltration amount for varying precipitation intensities.

3. Results and discussion

3.1. Idealized numerical experiments

Fig. 4**A** shows the range, interquartile range, and median value of total infiltration at varying precipitation intensities; the range shows the variability among 18 gauges across the study domain. As the precipitation intensity becomes greater, the median of total infiltration first increases rapidly, and then becomes steady. Because the precipitation input is only applied at the first hour of the simulation, so "precipitation intensity" is interchangeably used below as "precipitation amount". The one to one line in Fig. 4**A** represents the situation where 100% of precipitation is infiltrated. For lower precipitation intensities (less than 25.4 mm/hr), precipitation in all tested catchments is completely infiltrated – indicated by the total infiltration values aligning with the reference line. For greater precipitation intensities, variation in the catchments' total infiltration starts to emerge as indicated by the increased range and interquartile range. This is related to the combination of antecedent soil moisture, soil properties, geographical factors in various catchments starts to exhibit differences within increasing precipitation intensity. Nonetheless, soils in some catchments still take in most of the precipitation even at high precipitation intensities as indicated by the upper limit of total infiltration values. Similar to Fig. 4**A**, Fig. 4**B and 4C** show the same statistics (range, interquartile range, and median value) of local and re-infiltration for various precipitation intensities. In Fig. 4**B**, it is counter-intuitive for some local infiltration values to get below zero, which means that exfiltration occurred and runoff is thus greater than precipitation under the corresponding precipitation intensity and the "terrain-off" routing option. According to our approach of calculating re-infiltration (Section 2.4.1), the exfiltration condition causes the corresponding re-infiltration to be greater than total infiltration. Same as the case of total infiltration, greater precipitation intensities give rise to variations, or more precisely, heterogeneities among the catchments in local- and re-infiltration processes.

Fig. 5**A to 5C** show total infiltration, local infiltration, and re-infiltration values at various saturation levels of initial soil moisture in the first soil layer (0–10 cm). Similarly, Fig. 5**D to 5F and 5G to 5I** show the trends of total, local and re-infiltration in the second (10–40 cm) and third (40–100 cm) soil layers, respectively. It can be found that in all three soil layers, as initial soil moisture gets closer to saturation, total infiltration and local infiltration both slowly decrease, while re-infiltration slightly increases. This behavior of re-infiltration seems counterintuitive because one may expect soil layers of higher saturation levels would result in smaller amount of re-infiltration due to decreased soil storage for water to go in. However, it has to be understood that re-infiltration is simulated as a secondary process to local infiltration, where water routed from upstream cells being added to the excess runoff and then infiltrating. Higher antecedent soil moisture means decreased local infiltration, which leaves more water available for going downstream over the hillslopes and re-infiltrating subsequently. Overall, local infiltration is still the dominant pathway for infiltration while re-infiltration is a secondary effect. It is also found that all three types of infiltration are most sensitive to change of soil moisture in the third layer of soil possibly because of its greater thickness/storage compared to the upper two soil layers.

Fig. 6**A to 6C** show the total infiltration, local infiltration, and re-infiltration values at various terrain slope levels, respectively. While local infiltration is generally unaffected by terrain slope, the total- and re-infiltration both first decrease and then become stable as terrain becomes steeper. Note that local infiltration is calculated by only considering water transfer in the vertical columns of soil, plant, and atmosphere (in the Noah-MP LSM), thus it does not change as terrain slope changes. In comparison, re-infiltration is an augmented module by WRF-Hydro to describe the water loss during lateral water transfer pathways, therefore it can be influenced by terrain slope and thereby further influencing total infiltration amount. These results suggest that by neglecting re-infiltration, the effect of terrain slope on total infiltration may be underestimated. This is especially important to study domains with lower terrain slopes - the most obvious differences are seen for terrain slopes with smaller multipliers (less than 5). For steeper terrain slope ranges (multiplier greater than 5), faster overland flow rate is expected and therefore it gives less chance for water to re-infiltrate, which explains why limited effect is seen in steeper terrain slope conditions. In addition to the above, we also found that the ranges and interquartile ranges of the three types of infiltration are almost constant with varying terrain slopes across gauges. This is in contrast with Fig. 4 and Fig. 5 where the ranges are generally larger, indicating little interaction between terrain slope and other factors in affecting infiltration processes.

Fig. 7**A–C** show the trends of total, local and re-infiltration as saturated hydraulic conductivity (K_{sat}) changes, respectively. First, local infiltration is found to increase with greater K_{sat} because soil with higher K_{sat} is easier for water to pass through. Re-infiltration decreases with higher K_{sat} while total infiltration first increases rapidly and then becomes stable. The reason is that higher K_{sat} leads the majority of water to infiltrate locally, leaving less water to be re-distributed to downstream areas where re-infiltration occurs. In other words, water has a higher tendency or priority to infiltrate locally than re-infiltrate somewhere downstream. This finding is consistent with Niu et al. (2014) that larger K_{sat} facilitates surface water to infiltrate into deeper soils by gravity instead of flowing laterally. However, for soils with smaller K_{sat}, precipitation rate can readily exceed infiltration rate, which leaves more surface water for re-distribution and re-infiltration. In addition, for the three types of infiltration, the variation among tested catchments all decreases with greater K_{sat} values, as indicated by the decrease in the ranges. As K_{sat} increases, precipitation in any catchment is more likely to fully infiltrate via either local infiltration or

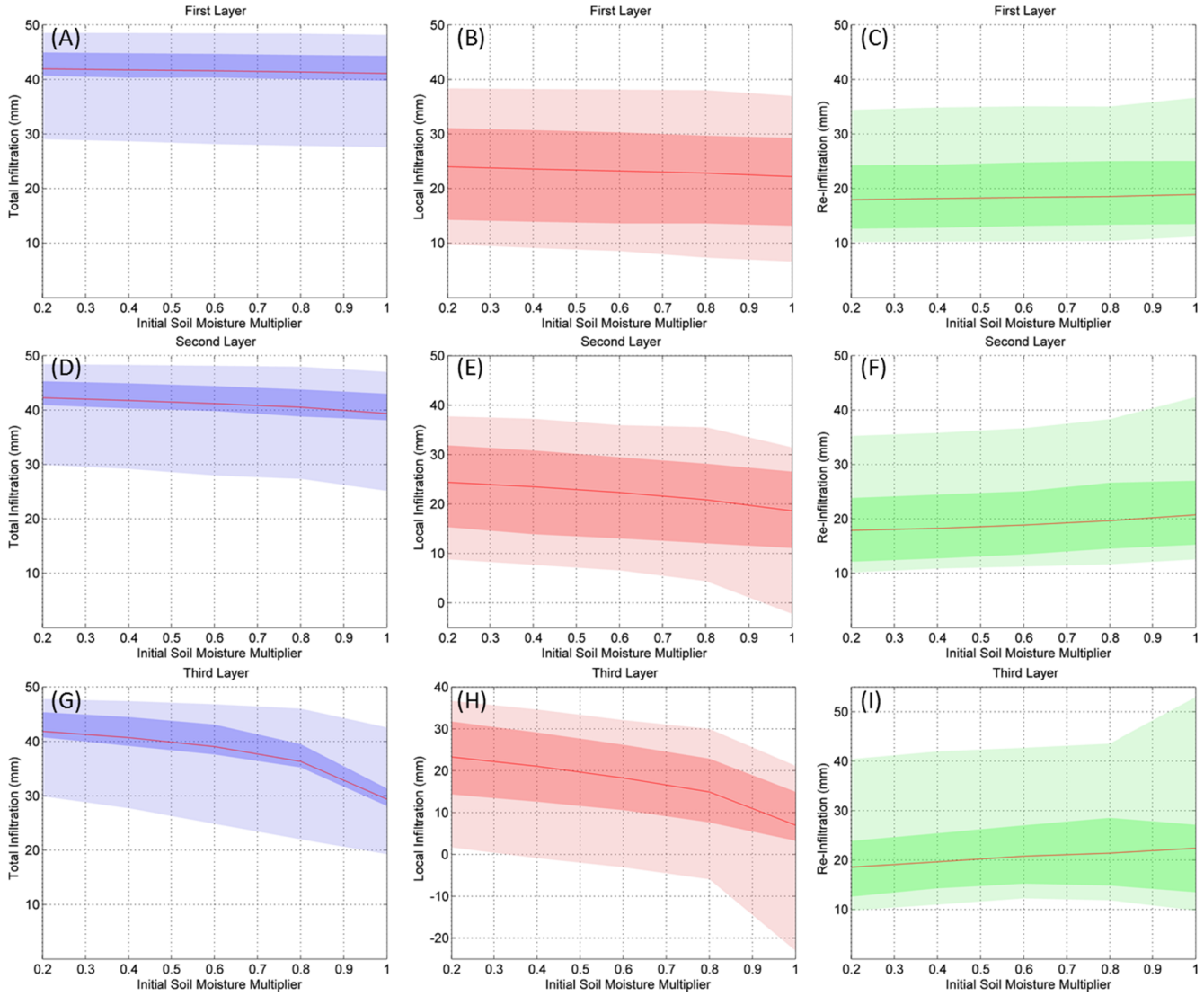

Fig. 5. . The range, interquartile range, and median value of different infiltration component for varying initial soil moisture conditions in different soil layers. (A)-(C) Total, local, and re-infiltration amount when changing initial soil moisture in first layer (0–10 cm); (D)-(F) Total, local, and re-infiltration amount when changing initial soil moisture in second layer (10 cm − 30 cm); (G)-(I) Total, local, and re-infiltration amount when changing initial soil moisture in third layer (30 cm − 100 cm).

re-infiltration or both. In essence, precipitation intensity, as the upper limit of infiltration rate, interacts with K_{sat} in affecting infiltration processes.

After testing five model parameters (RETDEPRTFAC, LKSATFAC, SLOPE, REFKDT, and OVROUGHRTFAC), we found that infiltration processes are only sensitive to REFKDT and OVROUGHRTFAC as shown in Figs. 8 and 9. Note that the REFKDT essentially controls the partition between surface and subsurface runoff, and greater REFKDT means less (more) surface (subsurface) runoff. Such an effect is evident in Fig. 8**B** where local infiltration increases with greater REFKDT, which is also

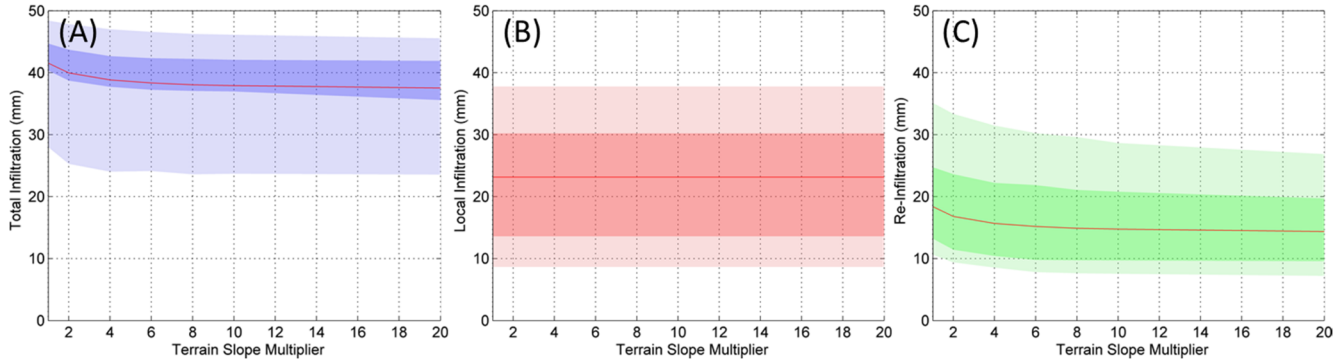

Fig. 6. . The range, interquartile range, and median value of (A) total infiltration, (B) local infiltration, and (C) re-infiltration amount for varying terrain slope.

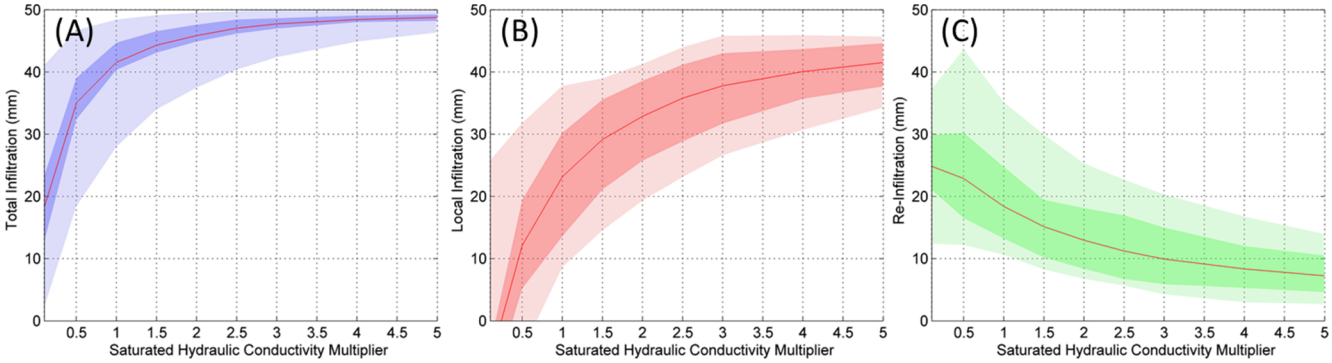

Fig. 7. . The range, interquartile range, and median value of (A) total infiltration, (B) local infiltration, and (C) re-infiltration amount for varying scale factor of saturated hydraulic conductivity.

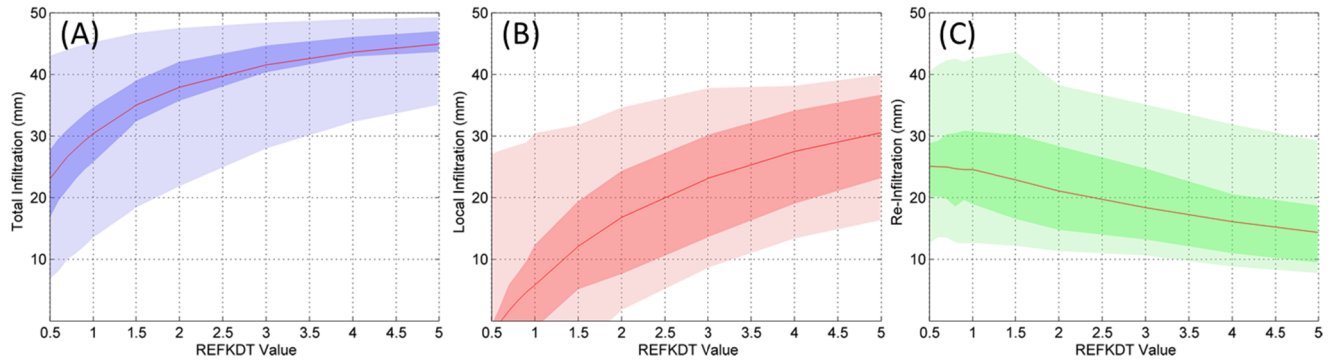

Fig. 8. . The range, interquartile range, and median value of (A) total infiltration, (B) local infiltration, and (C) re-infiltration amount for varying REFKDT value.

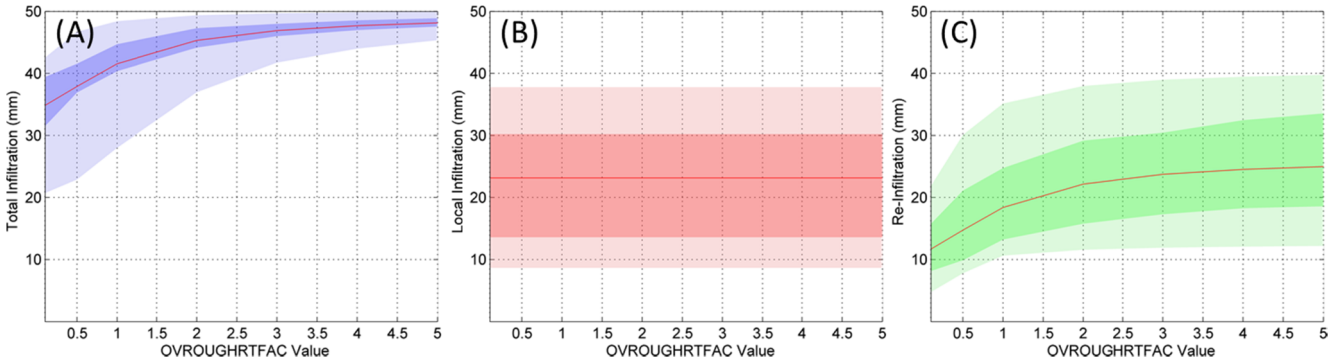

Fig. 9. . The range, interquartile range, and median value of (A) total infiltration, (B) local infiltration, and (C) re-infiltration amount for varying OVROUGHRTFAC value.

consistent with findings from previous studies (Schaake et al., 1996; Niu, 2011). Contrary to local infiltration, re-filtration decreases with greater REFKDT. As seen previously in Figs. 5 and 7, re-infiltration appears to be a secondary route for water to transfer into subsurface than local infiltration. The increasing trend of total infiltration flattens when REFKDT exceeds 3 (ranging from 0.5 to 5) due to the complete infiltration of precipitation. This is very similar to the case shown in Fig. 9**A:** greater OVROUGHRTFAC slows down the water transfer over hillslopes and retains the runoff for infiltration to the point where 100% of precipitation seeps into soils. In Fig. 9**B and 9C**, it is found that local infiltration is not affected by the OVROUGHRTFAC values, while re-infiltration first increases rapidly and then slowly with greater OVROUGHRTFAC. The reason is that rougher surfaces cause slower overland flow rate further giving water more chance to re-infiltrate.

In summary, based on the experiments above, a common finding is reached as follows. Local infiltration is a more direct route than re-infiltration through which water transfers down into soils. Under the principle of mass conservation, the changes in local and re-infiltration due to a single factor can be opposite to each other as seen in the cases of precipitation intensity (Fig. 4), initial soil moisture (Fig. 5), K_{sat} (Fig. 7), and REFKDT (Fig. 8). More (less) water infiltrating locally means less (more) water to re-distribute to downstream cells and re-infiltrate. Such observation makes more sense when variations of the three types of infiltration are examined (Figs. 7 and 8**)** among tested catchments: As the factor (K_{sat} or REFKDT) increases, total infiltration become less varied among the 18 catchments while variation of local- and re-infiltration remains steady. The common explanation is that the increasing factor causes precipitation to fully infiltrate in many catchments via both local- and re-infiltration, thus yielding the decreasing variation of total infiltration; and in these catchments where total infiltration is constrained, local- and re-infiltration yield the same sum though each bearing considerable variations among different catchments. When a factor only affects water transfer over the hillslopes instead of vertically, re-infiltration changes independently from local infiltration as seen in Fig. 6 and Fig. 9.

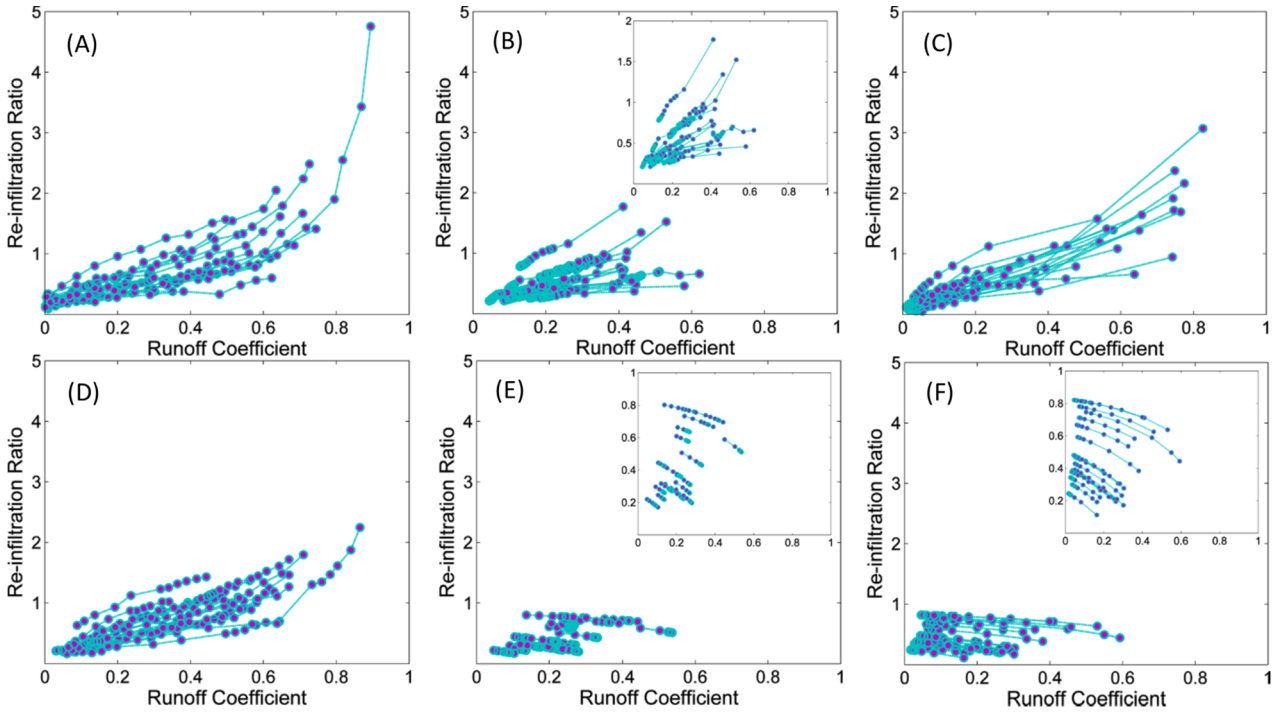

Fig. 10. . Trends of re-infiltration ratios for various runoff coefficients in different scenarios: (A) precipitation, (B) initial soil moisture, (C) saturated hydraulic conductivity, (D) REFKDT, (E) terrain slope, and (F) OVROUGHRTFAC. In each figure, one series of points is the result for one gauge and results of 18 gauges are plotted in total.

The experiments also highlight the factors that can lead to increased re-infiltration while having no effect on or decreasing local infiltration. For instance, mild terrain slope and lower K_{sat} results in more re-infiltration while local infiltration is unaffected or even less (Figs. 6 and 7). These results suggest that re-infiltration play an important role in hydrological processes for areas with flat terrain and clayey soils and thus needs to be sufficiently represented in hydrologic simulations. In order to better illustrate the portion of re-infiltration in total infiltration while assessing its relationship with flood potential, re-infiltration ratios and the corresponding runoff coefficients are shown in Fig. 10**A to 10F**. In Fig. 10, results from one catchment are plotted as one dotted line. In scenarios of varying precipitation intensities (Fig. 10**A**), initial soil moisture conditions (Fig. 10**B**), K_{sat} values (Fig. 10**C**), and REFKDT values (Fig. 10**D**), we can consistently see that re-infiltration ratio increases with greater runoff coefficient. Although with varying terrain slopes (Fig. 10**E**) and OVROUGHRTFAC values (Fig. 10**F**) re-infiltration ratios show a decreasing trend with a magnitude much smaller than the other cases. We further use box-plots (Fig. 11**A and 11B**) to summarize the variance of re-infiltration ratios and variance of runoff coefficients in response to changing factors. It is found that precipitation, K_{sat}, and REFKDT have higher impact on both re-infiltration ratio and runoff coefficient compared to the other factors, which confirms our earlier conclusions.

3.2. Real case simulation and calibration

Based on the above idealized modeling experiments, we choose 6 parameters for model calibration using DDS for the real-event simulation, which includes soil parameter K_{sat}, empirical runoff parameter REFKDT, scale factor of overland roughness OVROUGHRTFAC, and channel parameters (bottom width BtmWdth, side slope ChSlp, and Manning's roughness N). Figs. 12 and 13 show the comparisons of uncalibrated, calibrated and observed hydrographs at different gauge locations for 2010 Hermine and 2015 May Storm, respectively. The default parameterization (uncalibrated) is used to benchmark the calibration results because it represents the current setting in the operational NWM. Note that there is no available discharge observations at two gauges (ID: 08048800, 08056500) during 2010 Hermine and thus results from only 16 gauges are plotted in Fig. 12. After calibration, we can see great improvements at most gauges. Fig. 14 summarizes the CC, NSE, RMSE, and NBIAS statistics with boxplot. Our model calibration strategy brings CC and NSE much closer to 1, and RMSE and NBIAS much closer to 0. Improvement in RMSE and NBIAS indicates that calibration effectively corrected the underestimation of flow rates in the default simulation. The much narrower range of all four statistics also suggest that the calibration consistently improves the simulation performances at all tested gauges (Fig. 14). The satisfactory calibration enables us to quantify the re-infiltration amount with better assurance during different storm events and covering a wide range of locations, which would be otherwise difficult to obtain due to a lack of existing observation techniques.

To calculate re-infiltration in the calibrated simulation, another set of "terrain-off" simulations are conducted using the calibrated parameters in order to get values required by Eq. (3). Fig. 15 shows the relationship between runoff coefficients and re-infiltration ratios from all the testing catchments. It can be found that runoff coefficient and re-infiltration ratio are positively correlated, with the runoff coefficient ranging from 0 to 1. This is consistent with the idealized cases of varying precipitation, K_{sat}, initial soil moisture and REFKDT (see Fig. 10**A to 10D**). Compared to local infiltration, re-infiltration is simulated in WRF-Hydro as a secondary process, where water routed from upstream cells being added to the runoff excess and then infiltrating. However, re-infiltration can occur at a counter-intuitively faster rate than local infiltration (cases with re-infiltration ratio $>$ 50%) at basin-scale and event-scale. This is probably due to the faster overland flow rate generated in these cases. Scenarios with re-infiltration ratio being greater than one are noted, which possibly indicates that exfiltration would occur under terrain-off routing option. However, these six dots with seemingly unreasonable re-infiltration ratio are all from 2015 May event. To further investigate the possible reasons behind this, we examined the antecedent soil moisture and soil types (Fig. 16), where we found these exfiltration processes are generally

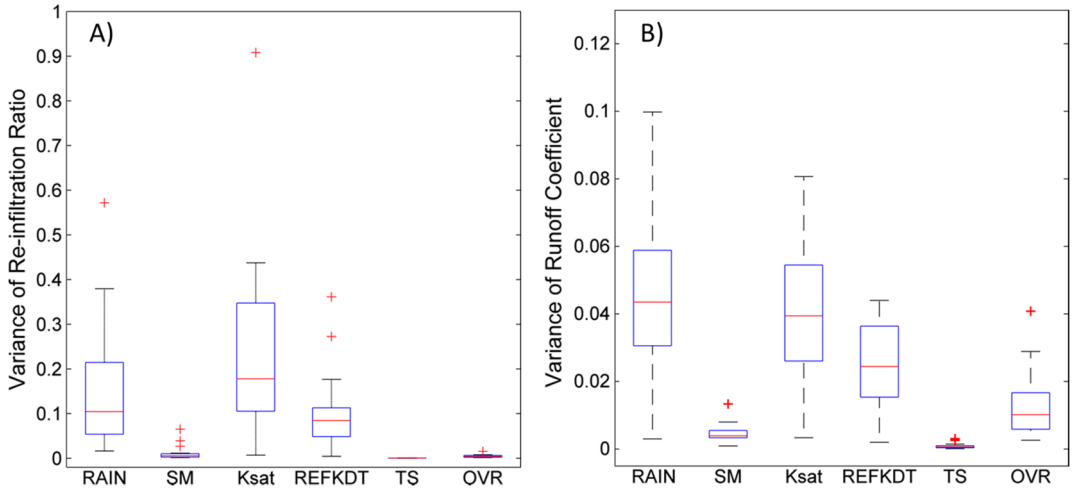

Fig. 11. . Box-plots of (A) variance of re-infiltration ratio (B) variance of runoff coefficient due to the change of different factors: precipitation (RAIN), soil moisture (SM), saturated hydraulic conductivity (Ksat), REFKDT, terrain slope (TS), and overland roughness (OVR).

occurred in sub-basins with two common features, i.e., clayey soils and high antecedent soil moisture (> 80% saturated in the top layer). Before our target event in May 2015, several storms occurred in North Central Texas, which have almost saturated the soil (Lin et al. 2018). These soil columns could very easily reach full saturation, and thus exfiltration may occur with much water contained in the soil storage. Without considering the re-infiltration process, the added amount of runoff from exfiltration would have no chance to enter the soils but to directly become streamflow in the channel. Should a calibration be conducted under such a circumstance (terrain-off), parameters could be wrongfully adjusted to compensate the missing re-infiltration process in WRF-Hydro.

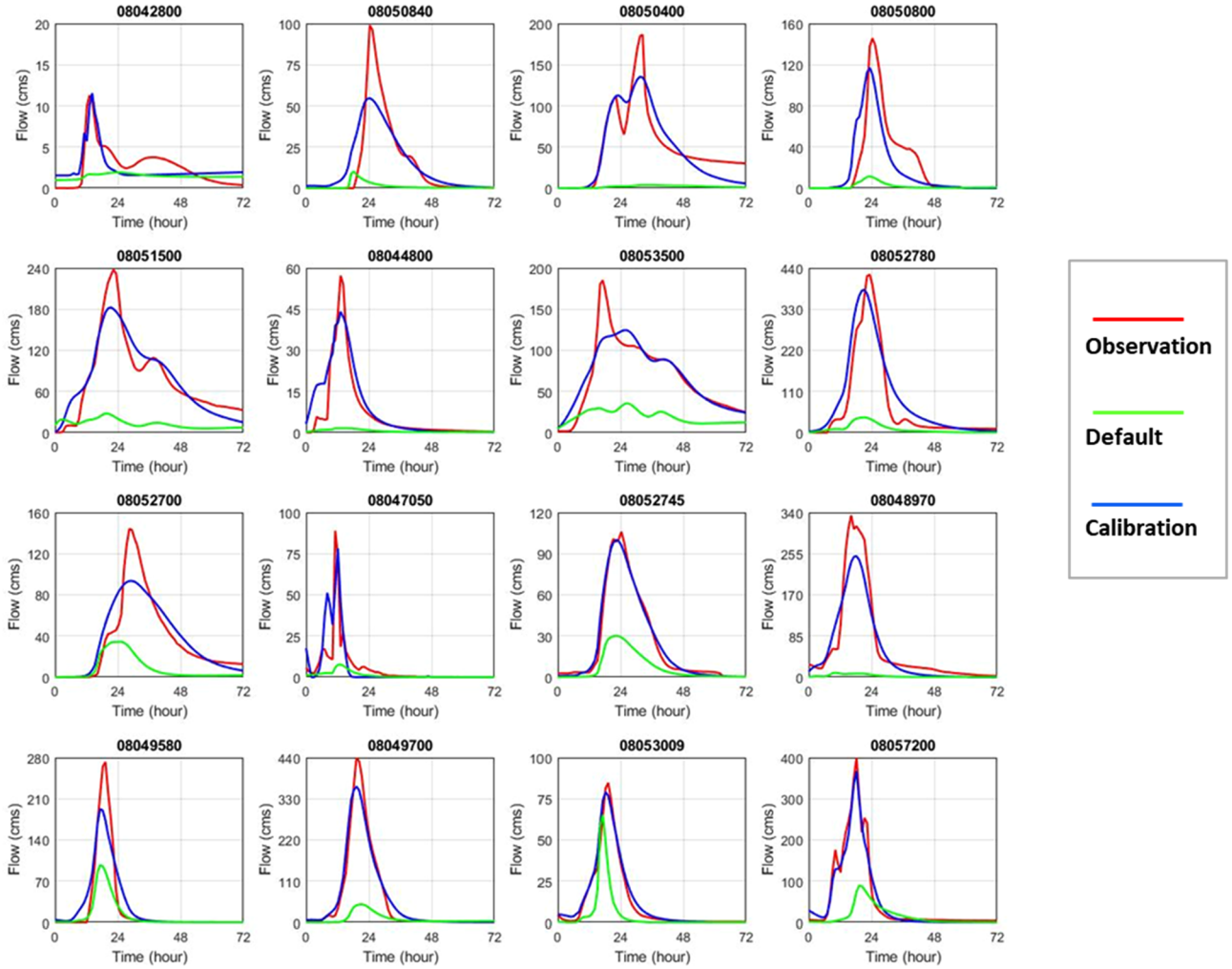

Fig. 12. . Calibration results of 2010 Tropical Storm Hermine for 16 gauges.

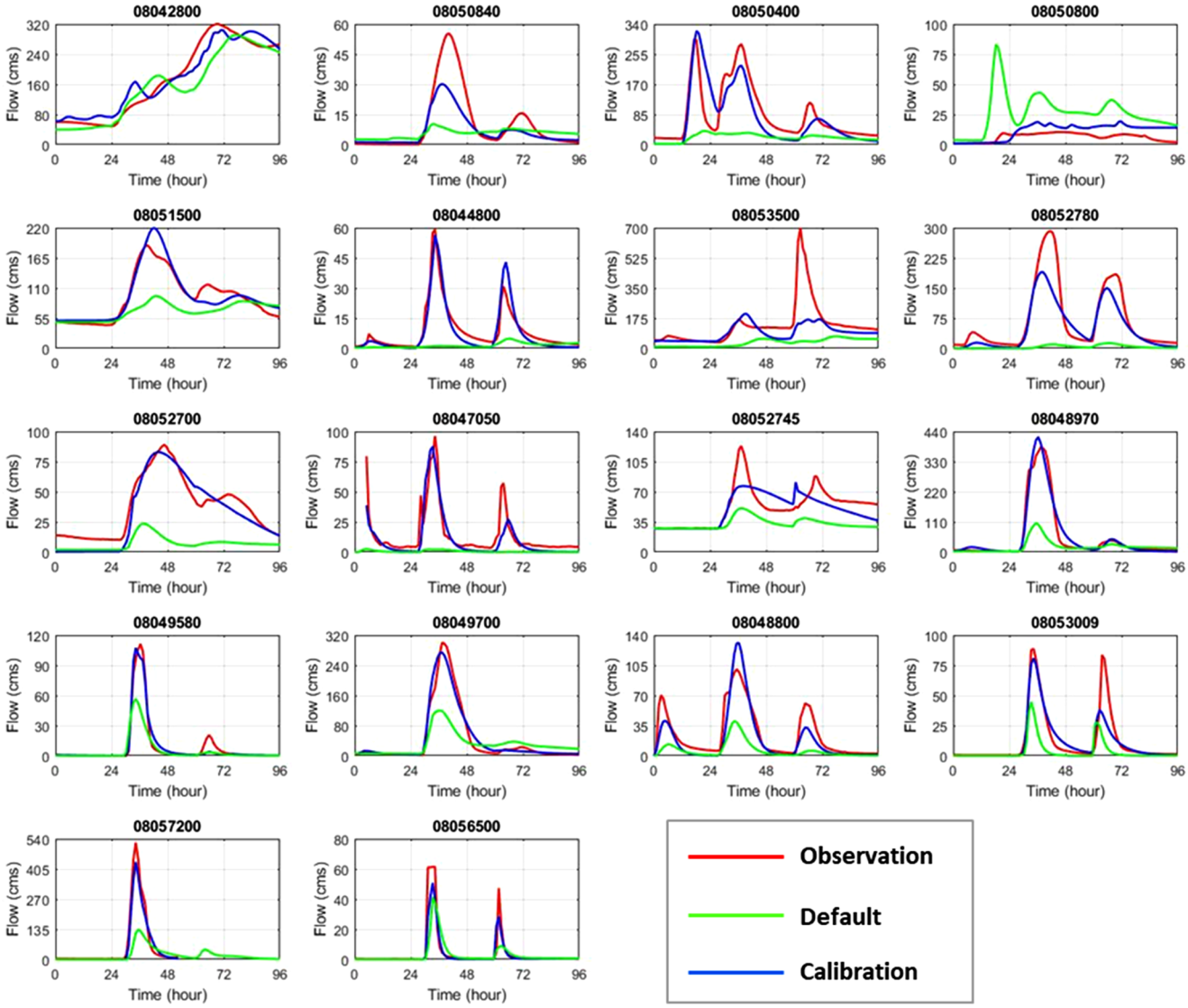

Fig. 13. . Calibration results of 2015 May Event for 18 gauges.

4. Conclusions

In this study, the authors leverage the physically-based and distributed WRF-Hydro modeling framework to comprehensively assess the re-infiltration process (also referred to as the "run-on" process in literature), a process often missing in traditional hydrologic models. In particular, we investigate the effects of hydrometeorological/geographical conditions and model parameters on re-infiltration simulations, aiming to provide a deeper understanding on re-infiltration than existing studies. Additionally, it is the first time that a detailed examination of the re-infiltration module in WRF-Hydro with different parameterization was provided. Using UTRB as the testbed, a group of idealized numerical experiments are first conducted to focus on individual factors while holding the others constant. The results not only reveal the pattern and magnitude of individual effects, but also inform the sensitivities of infiltration to each factor, providing guidance for the

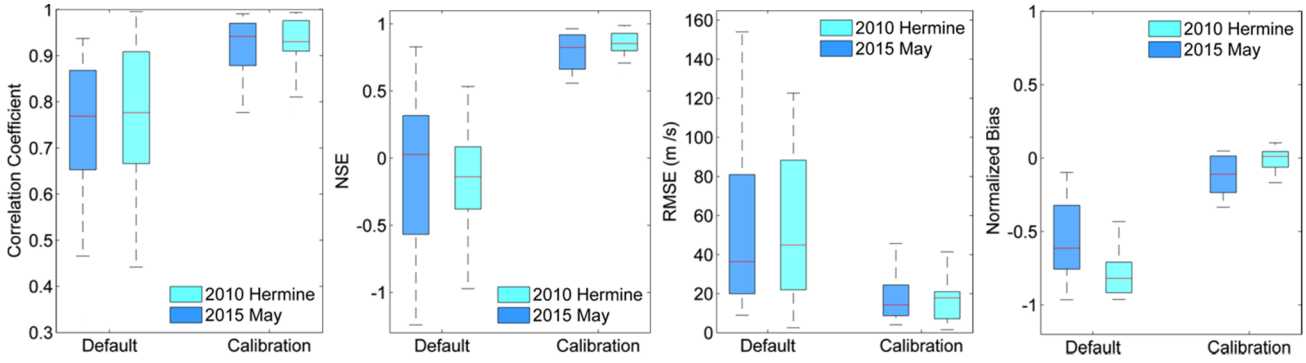

Fig. 14. . Before- and after-calibration statistics of 2010 Hermine (16 gauges) and 2015 May Event (18 gauges).

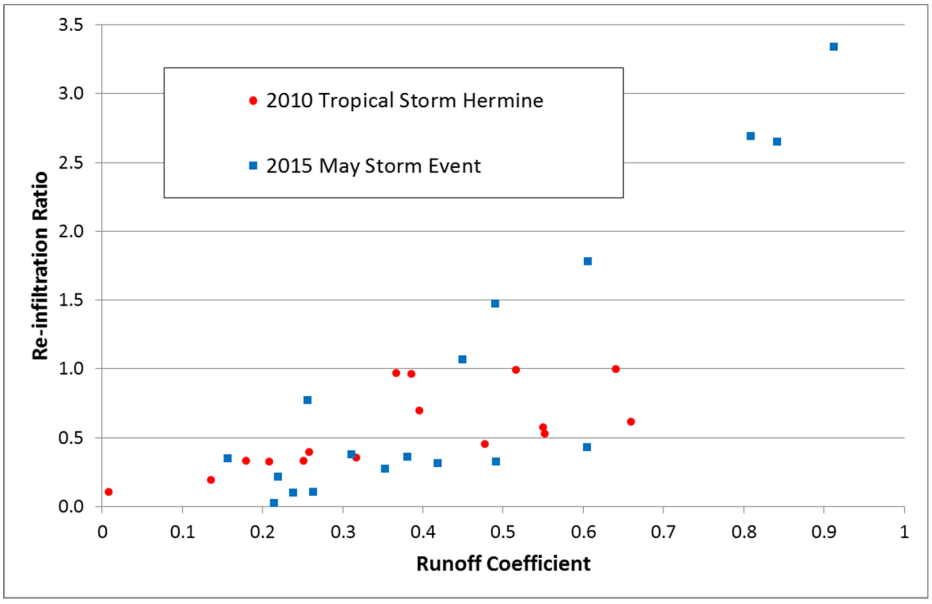

Fig. 15. . Trends of re-infiltration ratios for various runoff coefficients in two real events.

calibration effort in the subsequent analysis. In light of the idealized numerical experiments, two real storm events in UTRB are simulated and calibrated. Dominant factors to re-infiltration are identified from examining 18 sub-basins across the study area during these two events. In addition, the role of re-infiltration is investigated in relation with flood potential (indicated by runoff coefficient) to show the potential trade-offs in modeling re-infiltration for flood prediction purposes. The main conclusions from this study are summarized as follows:

1. Compared to local infiltration, re-infiltration is by nature a secondary process because of the preceding overland routing process; however, re-infiltration can occur at a counter-intuitively faster rate than local infiltration (cases with re-infiltration ratio $>$ 50%) at basin-scale and event-scale.

2. Under the principle of mass conservation, the changes in local and re-infiltration due to a single factor can be opposite to each other as seen in the cases of precipitation intensity, initial soil moisture, K_{sat} and REFKDT. More (less) water infiltrating locally means less (more) water to re-distribute to downstream cells and re-infiltrate.

3. The influence of re-infiltration on streamflow simulation can be substantial for areas with flat terrain and soil with high clay content (re-infiltration ratio is $>$ 50%).

4. Runoff coefficient and re-infiltration ratio are positively correlated, indicating that re-infiltration effects are more pronounced as flood potential increases and subsequently may be more important in urban than in rural regions.

For WRF-Hydro users, the insights gained from this study would be helpful for strategically choosing overland routing options based on the study domain's hydro-meteorological and graphical conditions. Given the computational cost for the terrain-on option and the complexity in considering related parameters in WRF-Hydro, users could potentially save time and resources while achieving satisfactory simulation results if re-infiltration is expected to be less influential. For modelers studying hydrology and hydrology-atmosphere feedbacks, understanding how different factors synergize or counteract with each other to affect re-infiltration is rewarding, as re-infiltration can play an indispensable role in the hydrologic cycle and in feeding back to the atmosphere. For instance, Senatore et al. (2015) concluded that accurate representation of re-infiltration improves precipitation simulation when fully coupled with WRF, suggesting the need to represent this important physical realism in the model. For the community of flood emergency responders, increasingly detailed and realistic representations of physical processes marks a shift in the paradigm of operational flood forecast from a past that heavily relies on human judgment/adjustment towards a computationally expensive but more robust future. Although re-

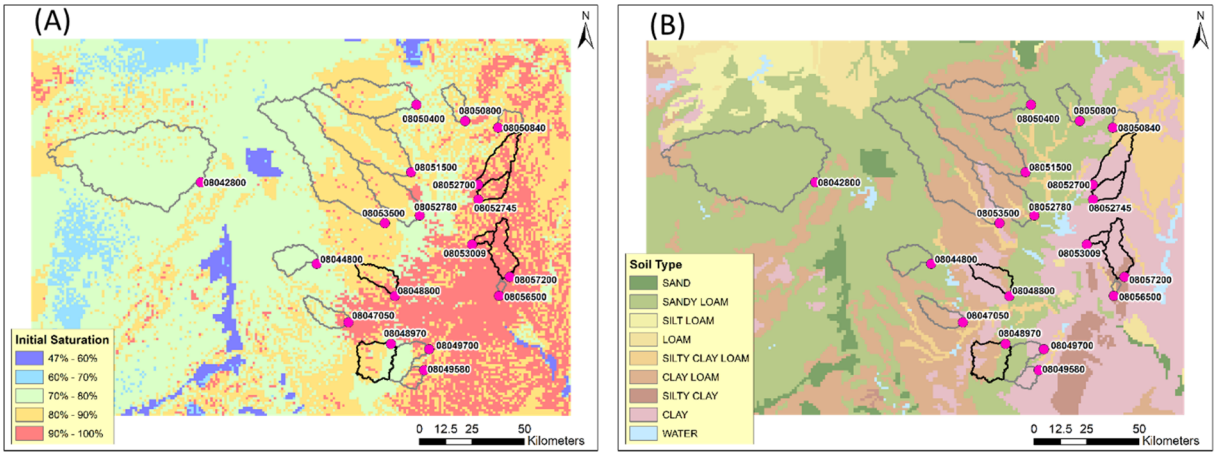

Fig. 16. . (A) Spatial pattern of the initial saturation level in the first layer soil (0–10 cm) at the beginning of 2015 May Event. (B) Soil type for 18 gauges in the study area. (Sub-basins with bold outlines are the ones with higher ($>$ 1) re-infiltration ratios).

infiltration was found significant for flood prediction in UTRB, it may prove to be a lesser process elsewhere. However, it is our emphasis that similar studies are imperative to elucidate the cost for missing or simplifying re-infiltration.

CRediT authorship contribution statement

Jiaqi Zhang: Conceptualization, Data curation, Formal analysis, Methodology, Investigation, Software, Validation, Writing - original draft, Writing - review & editing. **Peirong Lin:** Conceptualization, Formal analysis, Methodology, Investigation, Writing - review & editing. **Shang Gao:** Data curation, Formal analysis, Investigation, Visualization, Writing - review & editing. **Zheng Fang:** Supervision, Writing - review & editing.

Declaration of Competing Interest

The authors declare that they have no known competing financial interests or personal relationships that could have appeared to influence the work reported in this paper.

Acknowledgement

The authors would like to thank the funding support from the U.S. Army Corps of Engineers (Project number: W9126G-17-2-SOI-0977) and the National Science Foundation (Project number: 1832065). Special thanks to WRF-Hydro Training Workshop hosted by the National Center for Atmospheric Research (NCAR) and the Consortium of Universities for the Advancement of Hydrologic Science Inc. (CUAHSI). We also wanted to thank three anoymous reviewers and the editor for their suggestions to improve the quality of the manuscript.

References

Arnault, J., Wagner, S., Rummler, T., Fersch, B., Bliefernicht, J., Andresen, S., Kunstmann, H., 2015. Role of runoff-infiltration partitioning and additionally resolved overland flow on land-atmosphere feedbacks: a case study with the WRF-Hydro coupled modeling system for West Africa. J. Hydrometeorol. 17 (5), 1489–1516.

Borga, M., Anagnostou, E.N., Blöschl, G., Creutin, J.D., 2011. Flash flood forecasting, warning and risk management: the HYDRATE project. Environ. Sci. Policy 14 (7), 8.

Cai, X., Yang, Z.L., David, C.H., Niu, G.Y., Rodell, M., 2014. Hydrological evaluation of the Noah-MP land surface model for the Mississippi River Basin. J. Geophys. Res. Atmos. 119 (1) 23–38.34-844.

Corradini, C., Morbidelli, R., Melone, F., 1998. On the interaction between infiltration and Hortonian runoff. J. Hydrol. 204 (1–4), 52–67.

Corradini, C., Govindaraju, R.S., Morbidelli, R., 2002. Simplified modelling of areal average infiltration at the hillslope scale. Hydrol. Process. 16 (9), 1757–1770.

Deb, P., Babel, M.S., Denis, A.F., 2018. Multi-GCMs approach for assessing climate change impact on water resources in Thailand. Model. Earth Syst. Environ. 4 (2), 825–839.

Ek, M.B., Mitchell, K.E., Lin, Y., Rogers, E., Grunmann, P., Koren, V., Gayno, G., Tarpley, J.D., 2003. Implementation of Noah land surface model advances in the National Centers for Environmental Prediction operational mesoscale Eta model. J. Geophys. Res. Atmos. 108 (D22).

Fatichi, S., Ivanov, V.Y., Caporali, E., 2012. A mechanistic ecohydrological model to investigate complex interactions in cold and warm water-controlled environments: 1. Theoretical framework and plot-scale analysis. J. Adv. Model. Earth Syst. 4 (2).

Furl, C., Sharif, H., Zeitler, J.W., El Hassan, A., Joseph, J., 2018. Hydrometeorology of the catastrophic Blanco river flood in South Texas, May 2015. J. Hydrol.: Reg. Stud. 15, 90–104.

D.J. Gochis F. Chen Hydrological enhancements to the community Noah land surface model (No. NCAR/TN-454+STR) 2003 University Corporation for Atmospheric Research 10.5065/D60P0X00.

Gochis, D. J., Yu, W., Yates, D. N., 2013. The WRF-Hydro model technical description and user's guide, Version 1.0, NCAR Technical Document, 120 pp., NCAR, Boulder, Colo. Available online at: http://www.ral.ucar.edu/projects/wrf_hydro/.

D.J. Gochis J. Mc Creight W. Yu A. Dugger K. Sampson D.N. Yates A. Wood M. Clark R., 2015. Multi-scale water cycle predictions using the community WRF-Hydro modeling system. NCAR, Boulder, Colo. Available at https://ral.ucar.edu/sites/default/files/public/projects/wrf-hydro-modeling-system/1-wrf-hydro-v40-intro.pdf.

Gochis, D. J., Barlage, M., Dugger, A., FitzGerald, K., Karsten, L., McAllister, M., McCreight, J., Mills, J., RafieeiNasab, A., Read, L., Sampson K., , Yates, D., Yu, W., 2018. The WRF-Hydro modeling system technical description, Version 5.0. NCAR Technical Note. 107 pages. Available online at: https://ral.ucar.edu/sites/default/files/public/WRFHydroV5TechnicalDescription.pdf.

Gomi, T., Sidle, R.C., Miyata, S., Kosugi, K.I., Onda, Y., 2008. Dynamic runoff connectivity of overland flow on steep forested hillslopes: scale effects and runoff transfer. Water Resour. Res. 44 (8).

Gottschalk, L., Weingartner, R., 1998. Distribution of peak flow derived from a distribution of rainfall volume and runoff coefficient, and a unit hydrograph. J. Hydrol. 208 (3–4), 148–162.

Güntner, A., Bronstert, A., 2004. Representation of landscape variability and lateral redistribution processes for large-scale hydrological modelling in semi-arid areas. J. Hydrol. 297 (1–4), 136–161.

Gupta, H.V., Kling, H., Yilmaz, K.K., Martinez, G.F., 2009. Decomposition of the mean squared error and NSE performance criteria: Implications for improving hydrological modelling. J. Hydrol. 377 (1–2), 80–91.

Gupta, H.V., Kling, H., 2011. On typical range, sensitivity, and normalization of mean squared error and nash-sutcliffe efficiency type metrics. Water Resour. Res. 47 (10).

Heras, M.M.L., Nicolau, J.M., Merino-Martín, L., Wilcox, B.P., 2010. Plot-scale effects on runoff and erosion along a slope degradation gradient. Water Resour. Res. 46 (4).

IPCC (Intergovernmental Panel on Climate Change), 2014. Climate change 2014: synthesis report. Contribution of Working Groups I. II and III to the Fifth Assessment Report of the intergovernmental panel on Climate Change. IPCC, Geneva, Switzerland, 151.

Julien, P., Saghafian, B., Ogden, F.L., 1995. Raster-based hydrological modeling of spatially-varied surface runoff. Water Resour. Bull. 31 (3), 523–536.

Kerandi, N., Arnault, J., Laux, P., Wagner, S., Kitheka, J., Kunstmann, H., 2018. Joint atmospheric-terrestrial water balances for East Africa: a WRF-Hydro case study for the upper Tana River basin. Theor. Appl. Climatol. 131 (3–4), 1337–1355.

Lawrence, D.M., Oleson, K.W., Flanner, M.G., Thornton, P.E., Swenson, S.C., Lawrence, P.J., Zeng, X., Yang, Z.L., Levis, S., Sakaguchi, K., Bonan, G.B., 2011. Parameterization improvements and functional and structural advances in version 4 of the Community Land Model. J. Adv. Model. Earth Syst. 3 (1).

Lespinas, F., Dastoor, A., Fortin, V., 2018. Performance of the dynamically dimensioned search algorithm: influence of parameter initialization strategy when calibrating a physically based hydrological model. Hydrol. Res. 49 (4), 971–988.

Lin, P., Hopper Jr, L.J., Yang, Z.L., Lenz, M., Zeitler, J.W., 2018a. Insights into hydrometeorological factors constraining flood prediction skill during the May and October 2015 Texas Hill Country flood events. J. Hydrometeorol. 19 (8), 1339–1361.

Lin, P., Yang, Z.L., Gochis, D.J., Yu, W., Maidment, D.R., Somos-Valenzuela, M.A., David, C.H., 2018b. Implementation of a vector-based river network routing scheme in the community WRF-Hydro modeling framework for flood discharge simulation. Environ. Modell. Software 107, 1–11.

Lin, P., Rajib, M.A., Yang, Z.L., Somos-Valenzuela, M., Merwade, V., Maidment, D.R., Wang, Y., Chen, Li, 2017. Spatiotemporal evaluation of simulated evapotranspiration and streamflow over Texas using the WRF-Hydro-RAPID modeling framework. J. Am. Water Resour. Assoc. (JAWRA) 54 (1), 40–54.

Maidment, D.R., 2017. Conceptual framework for the national flood interoperability experiment. J. Am. Water Resour. Assoc. (JAWRA) 53 (2), 245–257.

Maneta, M.P., Silverman, N.L., 2013. A spatially distributed model to simulate water, energy, and vegetation dynamics using information from regional climate models. Earth Interact 17 (11), 1–44.

Morrs, R.E., 2010. Interactions among flood predictions, decisions, and outcomes: synthesis of three cases. Nat. Hazard. Rev. 11 (3), 83–96.

Nahar, N., Govindaraju, R.S., Corradini, C., Morbidelli, R., 2004. Role of run-on for describing field-scale infiltration and overland flow over spatially variable soils. J. Hydrol. 286 (1–4), 36–51.

NCTCOG iSWM, 2010. North Central Texas Council of Government integrated Stormwater Management Technical Hydrology Manual. Available online at: http://iswm.nctcog.org/Documents/technical_manual/Hydrology_4-2010.pdf.

G.Y. Niu., 2011. The community noah land-surface model (LSM) with multi-physics options. Tech. rep., National Centers for Environmental Prediction (NCEP), Oregon State University, Air Force, and Hydrology Lab–NWS, Available online at: https://www.jsg.utexas.edu/noah-mp/users-guide.

Niu, G.Y., Yang, Z.L., Mitchell, K.E., Chen, F., Ek, M.B., Barlage, M., Kumar, A., Manning, K., Niyogi, D., Rosero, E., Tewari, M., 2011. The community Noah land surface model with multiparameterization options (Noah-MP): 1. Model description and evaluation with local-scale measurements. J. Geophys. Res. Atmos. 116(D12).

Niu, G.Y., Troch, P.A., Paniconi, C., Scott, R.L., Durcik, M., Zeng, X., Huxman, T., Goodrich, D., Pelletier, J., 2014. An integrated modelling framework of catchment-scale ecohydrological processes: 2. The role of water subsidy by overland flow on vegetation dynamics in a semi-arid catchment. Ecohydrology 7 (2), 815–827.

NOAA (National Oceanic and Atmospheric Administration), 2016. National Water Model: Improving NOAA's Water Prediction Services. Available online at: http://water.noaa.gov/documents/wrn-national-water-model.pdf.

F.L. Ogden, 1997. CASC2D Reference Manual. Storrs, CT, University of Connecticut.

Qu, Y., Duffy, C.J., 2007. A semidiscrete finite volume formulation for multiprocess watershed simulation. Water Resour. Res. 43 (8).

Rigon, R., Bertoldi, G., Over, T.M., 2006. GEOtop: A distributed hydrological model with coupled water and energy budgets. J. Hydrometeorol. 7 (3), 371–388.

Saghafian, B., Julien, P.Y., Ogden, F.L., 1995. Similarity in catchment response, 1 Stationary rainstorms. Water Resour. Res. 31 (6), 1533–1541.

Senatore, A., Mendicino, G., Gochis, D.J., Yu, W., Yates, D.N., Kunstmann, H.G., 2015. Fully coupled atmosphere-hydrology simulations for the central Mediterranean: Impact of enhanced hydrological parameterization for short and long time scales. J. Adv. Model. Earth Syst. 7 (4), 1693–1715.

Schaake, J.C., Koren, V.I., Duan, Q.Y., Mitchell, K., Chen, F., 1996. Simple water balance model for estimating runoff at different spatial and temporal scales. J. Geophys. Res. Atmos. 101 (D3), 7461–7475.

Smith, R.E., Hebbert, R.H.B., 1979. A Monte Carlo analysis of the hydrologic effects of

spatial variability of infiltration. Water Resour. Res. 15 (2), 419–429.
Silver, M., Karnieli, A., Ginat, H., Meiri, E., Fredj, E., 2017. An innovative method for determining hydrological calibration parameters for the WRF-Hydro model in arid regions. Environ. Modell. Software 91, 47–69.
Sivapalan, M., Blöschl, G., Merz, R., Gutknecht, D., 2005. Linking flood frequency to long-term water balance: Incorporating effects of seasonality. Water Resour. Res. 41 (6).
Tolson, B.A., Shoemaker, C.A., 2007. Dynamically dimensioned search algorithm for computationally efficient watershed model calibration. Water Resour. Res. 43 (1).
USACE (U.S. Army Corps of Engineers), 2013. Corridor Development Certificate (CDC) – Upper Trinity River, Texas – Hydrologic and Hydraulic Model Update.
Wagener, T., Montanari, A., 2011. Convergence of approaches toward reducing uncertainty in predictions in ungauged basins. Water Resour. Res. 47 (6).
Wigmosta, M.S., Vail, L.W., Lettenmaier, D.P., 1994. A distributed hydrology-vegetation model for complex terrain. Water Resour. Res. 30 (6), 1665–1679.
Woolhiser, D.A., Smith, R.E., Giraldez, J.-V., 1996. Effects of spatial variability of saturated hydraulic conductivity on Hortonian overland flow. Water Resour. Res. 32 (3), 671–678.
Yair, A., Kossovsky, A., 2002. Climate and surface properties: hydrological response of small arid and semi-arid watersheds. Geomorphology 42 (1–2), 43–57.
Yair, A., Raz-Yassif, N., 2004. Hydrological processes in a small arid catchment: scale effects of rainfall and slope length. Geomorphology 61 (1–2), 155–169.
Z.L. Yang G.Y. Niu K.E. Mitchell F. Chen M.B. Ek Longuevergne Barlage L., Manning, K., Niyogi, D., Tewari, M. and Xia, Y., The community Noah land surface model with multiparameterization options (Noah-MP): 2. Evaluation over global river basins Journal of Geophysical Research Atmospheres 2011 116(D12).
Yucel, I., Onen, A., Yilmaz, K.K., Gochis, D.J., 2015. Calibration and evaluation of a flood forecasting system: Utility of numerical weather prediction model, data assimilation and satellite-based rainfall. J. Hydrol. 523, 49–66.
Zheng, H., Yang, Z.L., 2016. Effects of soil-type datasets on regional terrestrial water cycle simulations under different climatic regimes. J. Geophys. Res. Atmos. 121 (24), 14–387.